processes

MDPI

Article

A Distributionally Robust Optimization Strategy for a Wind–Photovoltaic Thermal Storage Power System Considering Deep Peak Load Balancing of Thermal Power Units

Zhifan Zhang and Ruijin Zhu *

College of Electrical Engineering, Tibet Agriculture and Animal Husbandry University, Nyingchi 860000, China
* Correspondence: zhuruijin@xza.edu.cn

Abstract: With the continuous expansion of grid-connected wind, photovoltaic, and other renewable energy sources, their volatility and uncertainty pose significant challenges to system peak regulation. To enhance the system's peak-load management and the integration of wind (WD) and photovoltaic (PV) power, this paper introduces a distributionally robust optimization scheduling strategy for a WD–PV thermal storage power system incorporating deep peak shaving. Firstly, a detailed peak shaving process model is developed for thermal power units, alongside a multi-energy coupling model for WD–PV thermal storage that accounts for carbon emissions. Secondly, to address the variability and uncertainty of WD–PV outputs, a data-driven, distributionally robust optimization scheduling model is formulated utilizing 1-norm and ∞-norm constrained scenario probability distribution fuzzy sets. Lastly, the model is solved iteratively through the column and constraint generation algorithm (C&CG). The outcomes demonstrate that the proposed strategy not only enhances the system's peak-load handling and WD–PV integration but also boosts its economic efficiency and reduces the carbon emissions of the system, achieving a balance between model economy and system robustness.

Keywords: thermal power unit deep peak shaving; combined WD–PV fire storage scheduling; distributionally robust optimization; synthetic norm constraint

Citation: Zhang, Z.; Zhu, R. A Distributionally Robust Optimization Strategy for a Wind–Photovoltaic Thermal Storage Power System Considering Deep Peak Load Balancing of Thermal Power Units. *Processes* **2024**, *12*, 534. https://doi.org/10.3390/pr12030534

Academic Editors: Qianzhi Zhang, Yujian Ye, Chong Wang, Dan Wu and Chunyu Chen

Received: 25 January 2024
Revised: 4 March 2024
Accepted: 5 March 2024
Published: 7 March 2024

1. Introduction

In recent years, China has seen a steady rise in its new energy installed capacity. According to the National Energy Administration's Demand Side Management for Peaking Coal power generation [1], China is striving to balance a secure and stable energy supply with sustainable, green, and low-carbon growth. This approach is in line with the country's methodical drive toward achieving carbon peak and carbon neutrality. The energy infrastructure in China has been progressively refined, boasting over 1.05 billion kilowatts of ultra-low emission coal-fired power generation units. Additionally, the share of clean energy consumption has climbed from 20.8% to surpass 25%, reflecting the nation's commitment to a more environmentally considerate energy mix.

China's energy resources are marked by a scarcity of oil and gas, with a notable abundance of coal. Wind (WD), photovoltaic (PV), and other clean energy sources are catching up at a relatively fast speed. China's installed coal power capacity will increase from 1.01 billion kilowatts in 2018 to 1.12 billion kilowatts in 2022, a net increase of only 110 million kilowatts. Renewable energy capacity surged from 728 billion kW in 2018 to 1.213 billion kW in 2022, constituting 47.3% of the total installed capacity. In 2022, China saw a historic moment as the total installed capacity of renewable energy surpassed that of coal power [1]. In the near future, new energy generation will become the main electricity supply. However, the high proportion of clean energy access for the stability of the power grid is a huge challenge. At the same time, we must also attach great importance to the consumption of new energy. The randomness, volatility, and uncertainty in renewable energy output pose inherent challenges to its consumption [2]; the system in the new energy

large-scale output and intermittent output peak–valley difference is large, and the peak load pressure continues to increase.

However, by the end of 2022, although the proportion of coal power capacity in China's total installed capacity dropped to about 43.8%, the proportion of electricity generation was still as high as 58.4% [1]. Currently, China's power system relies heavily on thermal power in its supply structure. The flexible adaptation of traditional thermal power units for deep peak regulation can greatly enhance the adjustment capacity on the power side [3]. Existing studies have shown that deep peak shaving is one of the most effective ways to boost renewable energy consumption in the flexible transformation of thermal power units [4–6]. At present, there have been many studies on deep peak shaving of thermal power units. Aiming at the phenomenon of power grid frequency fluctuation caused by the increasing proportion of renewable energy, Reference [7] proves the importance of deep peak regulation and on–off regulation for stabilizing system frequency through a series of derivations. In Reference [8], taking into account the extra coal consumption loss and unit life reduction of thermal power units operating in deep peak regulation without oil (DPR) mode, a robust optimization scheduling model of scale WD power grid-connected and DPR cost was proposed, and, finally, a robust day-ahead scheduling scheme with optimal economy was obtained. On the basis of thermal power storage, Reference [9] established a two-tier model involving hierarchical utilization of energy storage and DPR in the assistant service market, which can effectively improve the phenomenon of WD's abandonment and enhance the competitiveness of fossil power in the assistant service market of peak regulation. In Reference [10], proposing a unit commitment comprehensive optimal model aimed to minimize total costs by optimizing wind power curtailment in the context of the expensive deep peak regulation of thermal units. However, the above reference did not fully consider the probability distribution information of uncertain factors when optimizing the scheduling of uncertain outputs, such as WD and PV, which led to conservative optimization decision results and a poor economy. In order to address this issue, this paper incorporates the uncertainty of the probability distribution of WD and PV power output through the construction of fuzzy sets in day-ahead scheduling. To mitigate renewable energy abandonment, we leverage peak load balancing advantages, enhance clean energy absorption rates, and lower system operating costs.

Currently, two predominant research methodologies are employed to address the uncertainty inherent in integrating clean energy into the power system. These are stochastic optimization (SO) [11–14] and robust optimization (RO) [15–18]. Each method provides strategic frameworks for managing the unpredictable nature of clean energy outputs. Generally, SO necessitates a distribution model for uncertain parameters, which involves establishing numerous variables and constraints [14]. Given that the coefficient probability distributions are known, these constraints can be converted into deterministic ones for resolution. However, this often results in issues, such as an extensive computational scale and reduced efficiency in solving the model. The concept of RO is comparatively conservative, as it does not demand an accurate distribution model for uncertain parameters. Instead, the stochastic variability of the variables is characterized by a specified fluctuation boundary [19]. If the value of the variable remains within this boundary, an optimal solution can be derived using the robust optimization model [20]. Distributionally Robust Optimization (DRO), a data-driven approach, amalgamates the strengths of both SO and RO. It offers a novel solution paradigm that addresses the low precision of the SO model and the inherent conservatism of the RO model [21]. DRO constructs a set of uncertain probability distributions grounded in historical data and employs 1-norm and ∞-norm constraints over scenario probability distribution fuzzy sets. The aim is to ascertain the optimal solution under the premise that the prediction error of the uncertain factors adheres to the worst-case probability distribution [22]. This methodology adeptly circumvents the issue of nonlinear relationships inherent in indeterminate polynomials and the product of dual variables.

Similarly to the traditional two-stage robust optimization (TRO) solution, DRO also obtains the optimal solution of the problem through the iteration of the main problem and subproblem, but the TRO usually only considers the robustness, and the economy is poor; DRO takes robustness and economy into consideration through the iterative solution of the main subproblem and finally achieves the unity of robustness and economy.

Currently, distributionally robust optimization has found widespread application in the energy sector and integrated energy systems to accommodate renewable energy sources and minimize their impact on the energy grid [22,23]. However, its utilization in power systems remains limited. With the integration of large-scale renewable energy sources into power grids, conventional thermal power units are often compelled to shift from their traditional role as primary power suppliers to serving as auxiliary power sources to balance the fluctuating demand of the grid. Consequently, thermal power units may operate at peak loads for extended durations, leading to significant wear and tear on the units. Previous research indicates that energy storage systems can help alleviate the uncertainties associated with renewable energy [24].

Therefore, to alleviate the peak load on thermal power units and enhance the integration of renewable energy, this paper presents a distributionally robust optimization operation strategy of a WD–PV fire storage power system considering the deep peak shaving of thermal power units. Under the constraint of the comprehensive norm and considering the application of energy storage, to improve the absorption rate of renewable energy, a coordinated operation strategy of system robustness and a model economy is constructed. The main contributions of this paper are as follows:

(1) A fine modeling of a thermal power unit is carried out. By coupling energy storage equipment, the absorption rate of renewable energy is improved, and a distributionally robust optimal scheduling model of a thermal power unit coupled with WD and PV storage is established.

(2) The probability of uncertain scene distribution is constrained by combining 1-norm and ∞-norm, and the probability distribution of the worst scene is determined by updating the scene probability value.

(3) In order to maximize the consumption of new energy and reduce the abandonment of renewable energy, a collaborative optimization strategy of power system robustness and economy is established through comprehensive norm constraints. In addition, through the comparison of a variety of cases, the comprehensive effect of the model is verified.

The remainder of this paper is organized as follows: Section 2 introduces the peak-load model of the thermal power unit; Section 3 introduces the structure and operation strategy of the distributionally robust optimization model; and Section 4 introduces the optimization framework, data, and simulation results of the model. Section 5 provides a summary of the main discoveries, acknowledges limitations, and proposes future research directions.

2. Peak-Load Model of the Thermal Power Unit

In the power system with multiple thermal power units, especially when there are significant changes in power load or the integration of new energy sources, two typical modes of peak regulation operations emerge: deep peak regulation and on–off peak regulation.

2.1. Depth Peak Shaving of Thermal Power Units

Deep peak shaving in thermal power units involves modifying their output to match fluctuations in the integration of new energy sources. This adjustment aims to align with the output of wind and photovoltaic power generation, ensuring the real-time balance of system power [25].

Based on the operational status and energy consumption traits of thermal power units, the peak regulation process can be categorized into three modes: regular peak regulation (RPR), deep peak regulation without oil (DPR), and deep peak regulation with oil (DPRO). Relevant modes of depth peak shaving are shown in Figure 1.

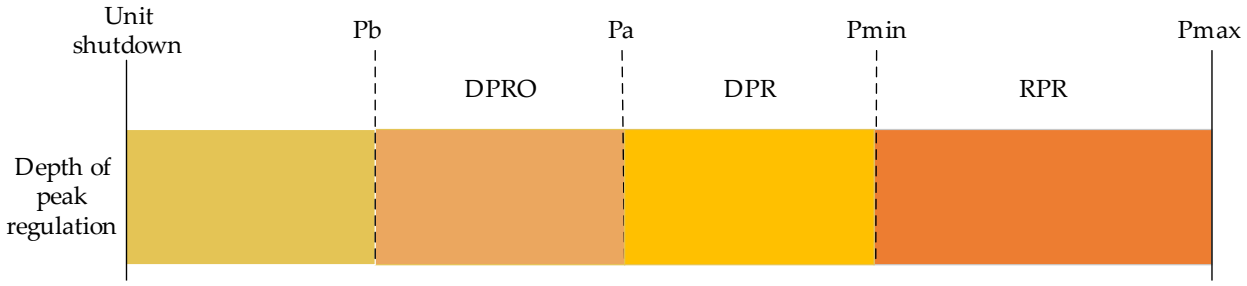

Figure 1. Peak regulation process for the thermal power unit.

Among them, Pb refers to the minimum operating output of the unit, Pa refers to the limit output of stable combustion of the unit during deep peak regulation, Pmin refers to the limit output of stable combustion of the unit during DPRO, and Pmax refers to the maximum operating output of the unit.

With the integration of large-scale, new energy sources into the power grid, the design considerations for 600 MW and 1000 MW high-capacity thermal power units emphasize the necessity of possessing a certain peak load capacity. Earlier investments in smaller-capacity thermal power units below 300 MW in China were constrained by technological limitations, enabling only base load capacity. At present, these smaller-capacity units have yet to undergo comprehensive transformation, resulting in slower responsiveness during depth peak regulation. Following the transformation of thermal power units, grid companies have significantly enhanced the depth of peak regulation, gradually augmenting the flexibility of these units to engage in deep peak regulation during periods of high demand for grid regulation [26]. However, the deep peak shaving operation of modified coal-fired power units deviates from their rated optimal operation, leading to performance deterioration in subsystems and auxiliary equipment [27]. Consequently, this gives rise to issues, such as a significant reduction in unit lifespan, elevated coal consumption costs, and increased carbon emissions within the power supply. The costs associated with peak regulation for thermal power units can be broadly categorized into coal consumption cost, shaft life cost, and oil injection cost.

(1) Coal consumption cost of the thermal power unit.

The coal consumption cost of thermal power units is usually expressed by consumption characteristics. A fixed set of abc coefficients [28] is usually adopted for specific units participating in generation optimization scheduling. The coal consumption characteristic parameters of thermal power units can be obtained through function fitting. The coal consumption cost of units participating in peak load balancing can be shown in Equation (1):

$$C_1 = (a_i P_{gi.t}^2 + b_i P_{gi.t} + c_i) C_{coal} \quad (1)$$

where C_1 represents the coal consumption cost of the thermal power unit i at t moment, $P_{gi.t}$ represents the actual output power of the thermal power unit, C_{coal} represents the price (RMB/t) of coal purchased from the thermal power plant, and a_i, b_i, c_i represent the characteristic parameters for coal consumption in the thermal power unit i.

(2) Life cost of the rotating shaft

The steam turbine stands as the primary power generation equipment within a thermal power station, serving as the core component in most thermal power units. Its operation encompasses variable and fixed operating conditions. During transitions like start-ups and shut-downs, significant changes occur in steam temperature, pressure, and other parameters, leading to uneven heating of the rotor and primarily causing low-cycle fatigue damage. In contrast, when the steam turbine operates under fixed conditions, the metallic material comprising the rotor tends to gradually deteriorate due to thermal stress in high-temperature environments, leading to damage primarily induced by high-temperature

creep [29]. Throughout operation, both low-cycle fatigue damage and high-temperature creep damage typically manifest simultaneously. Coupled with varying capacities across different thermal power units, the life loss of the rotor shaft is exacerbated. This paper calculates the rotor shaft's lifespan cost using the Manson–Coffin formula as a reference, expressing its life cost through Equations (2) and (3):

$$C_2 = \frac{\lambda C_{unit}}{2N_f(P_{gi.t})} \tag{2}$$

$$\begin{aligned} N_f(P_{gi.t}) = \quad & 0.00577P_{gi.t}^3 - 2.682P_{gi.t}^2 \\ & +484.8P_{gi.t} - 8411 \end{aligned} \tag{3}$$

where C_2 denotes the thermal power unit i in the depth peak load, the life cost of the rotating shaft at t time, $N_f(P_{gi.t})$ represents the function of the cracking cycle of the rotor on the actual output power [6], and C_{unit} represents the construction cost (RMB/MW) of the thermal power unit.

(3) Cost of fuel injection

During the oil injection deep peak shaving phase of a thermal power unit, the combustion of coal within the unit experiences instability. Injecting oil into the boiler becomes necessary to facilitate static coal burning, thereby ensuring the stable operation of both the boiler and the unit's water cycle. The oil injection cost for the thermal power unit can be expressed using Formula (4):

$$C_3 = Q_{oil}S_{oil} \tag{4}$$

In Formula (4), C_3 represents the oil cost of the thermal power unit i in the depth peak load at t time, Q_{oil} represents the fuel consumption of the thermal power unit in the DPRO stage, and S_{oil} represents the price of unit oil.

In conclusion, the cost of deep peak shaving for thermal power units can be represented using a piecewise function (5):

$$C(P_{gi.t}) = \begin{cases} C_1 & P_{\min} \le P_{gi.t} \le P_{\max} \\ C_1 + C_2 & P_a \le P_{gi.t} \le P_{\min} \\ C_1 + C_2 + C_3 & P_b \le P_{gi.t} \le P_a \end{cases} \tag{5}$$

(4) Analysis of carbon emissions in the peak regulation process

The calculation of carbon emissions of thermal power units in the process of peak load balancing is the basis of realizing low-carbon scheduling of a power system. At present, the carbon emission calculation methods for power system scheduling mainly include three methods.

It is approximately considered that the carbon emission of thermal power units is proportional to its output, and the proportional coefficient is carbon emission intensity [30]. This method is simple and clear, and it has been adopted in most references.

Polynomial functions similar to unit consumption characteristics are used for fitting, such as quadratic function [31], cubic function [32], etc.

The power supply unit's coal consumption is multiplied by the carbon dioxide emission coefficient [33].

In this study, the quadratic function in the second method is employed to model carbon emissions in the peak shaving process, so the process can be expressed by Equations (6) and (7):

$$C_{emi} = C_{emi.g} + C_{emi.b} \tag{6}$$

$$\begin{cases} C_{emi.g} = \sum_{t=1}^{T}\sum_{i=1}^{N}\left[\alpha_i(P_{gi.t})^2 + \beta_i P_{gi.t} + \lambda_i\right] \\ C_{emi.b} = H\sum_{t=1}^{T} P_{\text{buy.t}} \end{cases} \tag{7}$$

where C_{emi}, $C_{emi.g}$, and $C_{emi.b}$, respectively, represent the total carbon emissions of the power system, the carbon emissions of thermal power units in the peak load balancing process, and the equivalent carbon emissions of the system to the power grid, α_i, β_i and λ_i, respectively, represent the carbon emission characteristic function parameters of unit i, and H denotes the equivalent carbon emission characteristic function parameters of power purchase.

In the actual peak shaving process, the involved devices include electric energy storage and WD–PV power generation. Given that wind power and photovoltaic systems operate on clean energy sources, their carbon emissions are not factored into the actual power generation process. Additionally, the charge and discharge process of energy storage primarily involves internal chemical reactions devoid of carbon emissions. Hence, this paper disregards the consideration of carbon emissions from electric energy storage, wind power, and photovoltaic sources.

2.2. Thermal Power Unit On–Off Peak Regulation

On–off regulation in thermal power units refers to a process where, in the event of a significant increase or decrease in renewable energy penetration or a heightened load peak–valley difference within the power system, merely employing depth peak load regulation becomes insufficient for the thermal power unit to maintain the system's power balance. Consequently, expanding the peak regulation scope necessitates the adjustment of the number of connected thermal power units to the grid, either reducing or increasing them.

On–off peak regulation stands as a primary method for thermal power units to engage in peak regulation. Units operating under variable conditions not only impact the lifespan of the rotor shaft but also induce irreversible changes in other metallic components of the unit. These alterations affect the unit's overall service life, resulting in on–off costs. The cost associated with unit participation in on–off peak shaving can be represented by Equations (8) and (9):

$$C_4 = V_{gi.t}(1 - V_{gi.t-1})C_{iup} + V_{gi.t-1}(1 - V_{gi.t})C_{idown} \tag{8}$$

$$V_{gi.t} = L_{gi.t} + J_{gi.t} + K_{gi.t} \tag{9}$$

In the formula, C_4 denotes the on–off cost of the unit, $V_{gi.t}$ denotes the binary state variable of the unit in the peak load phase, $L_{gi.t}$ denotes whether the unit is in the 0–1 state variable of RPR, $J_{gi.t}$ denotes whether the unit is in the 0–1 state variable of DPR, $K_{gi.t}$ denotes whether the unit is in the 0–1 state variable of DPRO, C_{iup} denotes the cost of the unit when it is started, and C_{idown} denotes the cost of the unit when it stops running.

Due to the high requirements of the reaction speed and the on–off time of the unit, the unit with small capacity and a short downtime is generally selected as the thermal power unit with on–off peak regulation [6].

3. Data-Driven Distributionally Robust Optimal Scheduling Model

With the integration of large-scale new energy sources like wind power into the grid, acknowledging their volatility and uncertainty becomes crucial due to their impact on the power system. Previously, many attributed the abandonment of wind power to technical challenges, citing issues with volatility, uncontrollability, and a lack of grid flexibility for WD and PV power generation. However, in the current context, the abandonment rates, reaching up to 30% to 40%, cannot be solely ascribed to technical limitations. The primary root cause lies in the scenario of excessive installed power capacity and oversupply, posing the challenge of determining priority usage among available resources. Although the Renewable Energy Law [34] mandates that renewable energy sources have priority access to the grid, the de facto priority in the current power system remains with thermal power generation. This priority status stems from the government's annual issuance of planned electricity quantities, which has constrained the developmental space for renewable energy. Consequently, to enhance the absorption capacity of wind and photovoltaic power stations

and address the uncertainties in their output alongside the adverse effects of forecast errors on the power system, this paper endeavors to construct a novel distributionally robust planning and scheduling strategy for WD–PV fire storage based on comprehensive norms. The schematic diagram of the system is shown in Figure 2.

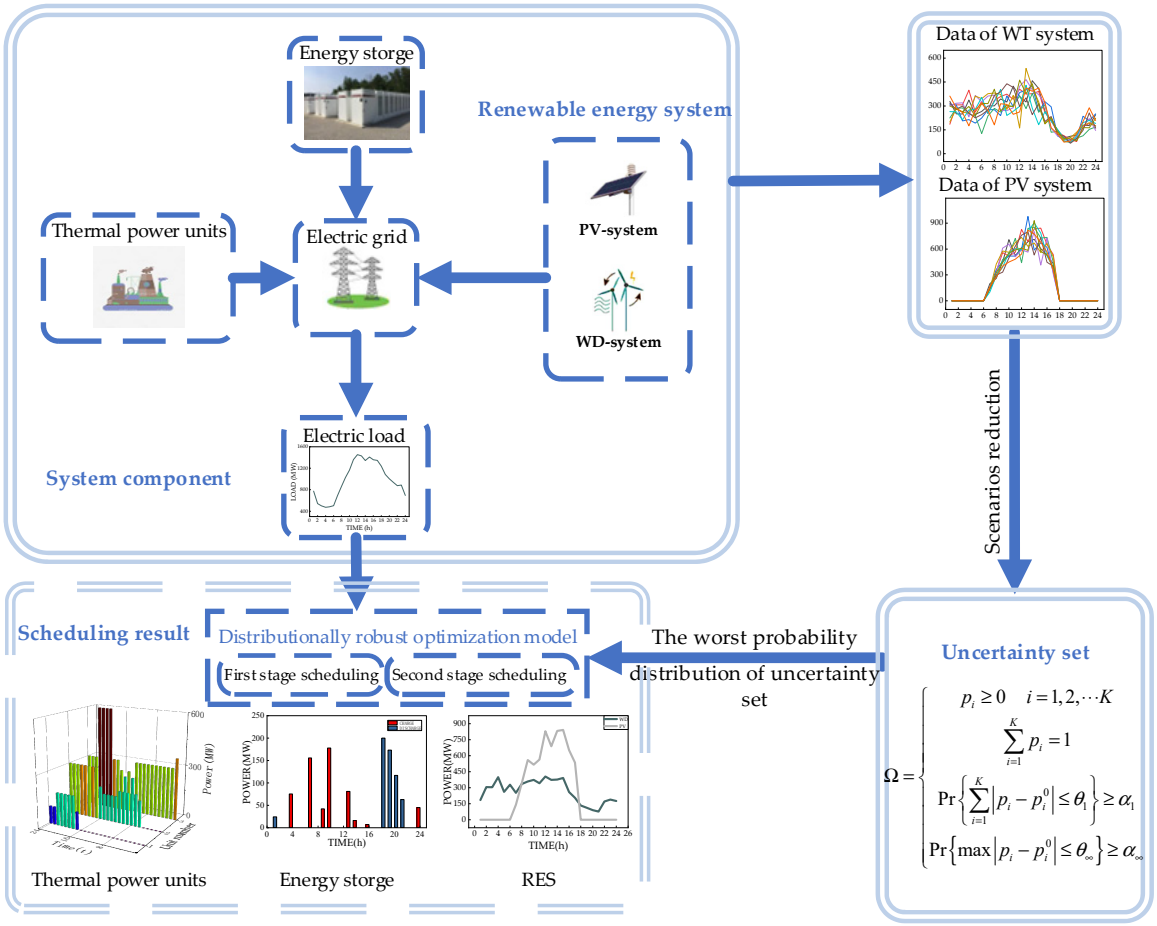

Figure 2. The schematic diagram of the power system.

3.1. Two-Stage Distributionally Robust Optimization Objective Function

In short-term day-ahead scheduling, the uncertainty associated with WD and PV power generation can be characterized by their output prediction errors. However, this method has limitations when applied to long-term scheduling. This paper aims to devise an optimal scheduling scheme considering the given prediction intervals for renewable energy. It seeks to achieve a cooperative optimization aligning system economy and robustness. Following the framework outlined in Reference [22], the objective function for the distributionally robust optimization is constructed as follows:

$$\min\left\{C_{stage1} + \max(p^{T+1}\min C'_{stage2})\right\} \tag{10}$$

where p^T represents the probability value of the generation scenario T, $T \geq 1$, C_{stage1} represents the power purchase cost of the system, and C'_{stage2} represents the operating cost of the unit during peak load balancing.

As evident from Equation (10), the objective function takes the form of a two-stage min–max–min robust optimization. Different from TRO, DRO solves the one-stage scheduling scheme in the worst case by optimizing the lower-bound LB and estimating its economy by $\min C'_{stage2}$. In the additional stage of the system, the "worst" scenario that the system may encounter is determined by $\max(p^{T+1}\min C'_{stage2})$ and the probability value is updated; the

unity of robustness and economy is realized through continuous iteration in the first and second stages.

The sub-function comprises power purchase costs and operating expenses. The operating costs encompass various elements: coal consumption costs during thermal power unit peak shaving, on–off costs, shaft life expenses, oil injection expenses, deep peak shaving compensation expenses, electric energy storage utilization costs, and wind and photovoltaic abandonment expenses. The expression is as follows:

$$C_{stage1} = S_{buy} P_{buy} \tag{11}$$

$$C'_{stage2} = C_{g1} + C_{g2} + C_{g3} - C_{GP} + C_{ES} + C_{cur} \tag{12}$$

In Formula (11), C_{stage1} is the power purchase cost of the thermal power unit during deep peak shaving, S_{buy} represents the purchase price of a large power grid (RMB/kWh), and P_{buy} represents the power purchased by the system from a large power grid during peak regulation. In Formula (12), C_{g1}, C_{g2}, and C_{g3}, respectively, represent the power generation cost of thermal power unit 1, unit 2, and unit 3, C_{GP} represents the compensation for the unit involved in deep peak regulation, C_{ES} represents the use cost of electric energy storage, and C_{cur} represents the penalty cost of abandoning renewable energy.

(1) Cost of power generation for the thermal power unit.

$$\begin{cases} C_{g1} = C_1 + C_4 \\ C_{g2} = C_1 + C_4 \\ C_{g3} = C_1 + C_2 + C_3 + C_4 \end{cases} \tag{13}$$

(2) Depth peak load compensation cost

$$C_{GP} = P_{gi.t} S_b \tag{14}$$

where S_b indicates the electricity compensation price.

(3) The cost of storing electric energy

$$C_{ES} = \delta_{ES} \sum_{t=1}^{24} (P^t_{ES.cha} + P^t_{ES.dis}) \tag{15}$$

where $P^t_{ES.cha}$ represents the charge power of the energy storage, $P^t_{ES.dis}$ represents the discharge power of the energy storage, and δ_{ES} represents the unit power of the electric storage cost.

(4) The curtailment of abandoning WD and PV

$$C_{cur} = \delta_{cur} \sum_{t=1}^{24} (P_{pv.cur} + P_{wd.cur}) \tag{16}$$

where $P_{pv.cur}$ denotes the amount of PV curtailment, $P_{wd.cur}$ denotes the amount of WD curtailment, and δ_{cur} denotes the cost of abandoning WD and PV per unit power.

3.2. Power Constraints

(1) System constraints

$$P_{g1} + P_{g2} + P_{g3} + P_{pv} + P_{wd} + P_{ES.dis} + P_{buy} = P_L + P_{ES.dis} \tag{17}$$

where P_L indicates the electrical load of the system.

(2) Unit constraints

The upper and lower limits of unit output constraints are

$$P_{gi.\min} \le P_{gi} \le P_{gi.\max} \tag{18}$$

where $P_{gi.\min}$ and $P_{gi.\max}$, respectively, represent the minimum and maximum technical outputs of thermal power units.

The unit climbing power constraint is

$$P_{gi.down} \le P_{gi}^{t} - P_{gi}^{t-1} \le P_{gi.up} \tag{19}$$

where $P_{g1.down}$ and $P_{g1.up}$, respectively, represent the maximum upward and downward climbing rates of thermal power units.

Unit on–off constraint

$$\begin{cases} V_{g1.\tau} \ge \tau(V_{g1.t} - V_{g1.t-1}) & \tau = t, t+1, t+2, \ldots, t + T_{g1.\min}^{on} - 1 \\ 1 - V_{g1.\tau} \ge \tau(V_{g1.t-1} - V_{g1.t}) & \tau = t, t+1, t+2, \ldots, t + T_{g1.\min}^{off} - 1 \end{cases} \tag{20}$$

where τ denotes the min continuous on–off time for units.

(3) Constraints of electric energy storage equipment

$$\begin{cases} P_{ES}^{\min} \le P_{ES}^{t} \le P_{ES}^{\max} \\ P_{ES.cha}^{\min} \le P_{ES.cha}^{t} \le \alpha_{H.cha} P_{ES.cha}^{\max} \\ P_{ES.dis}^{\min} \le P_{ES.dis}^{t} \le \alpha_{H.dis} P_{ES.dis}^{\max} \\ \alpha_{H.cha} + \alpha_{H.dis} \le 1 \\ P_{ES}^{t=1} = P_{ES}^{t=24} \\ P_{ES}^{t} = P_{ES}^{t-1} + \eta_{ES}^{cha} P_{ES.cha}^{t} - P_{ES.dis}^{t} / \eta_{ES}^{dis} \\ (2 \le t \le 24) \end{cases} \tag{21}$$

where P_{ES}^{t} represents the real-time capacity of electric energy storage, $P_{ES}^{\max}$ and $P_{ES}^{\min}$ represent the upper and lower limits of electric energy storage capacity, $\alpha_{H.cha}$ represents the charging state parameters of electric energy storage, $\alpha_{H.dis}$ represents the discharge state parameters of electric energy storage, $P_{ES.cha}^{\max}$ and $P_{ES.cha}^{\min}$, respectively, represent the upper and lower limits of the energy storage charging power, $P_{ES.dis}^{\max}$ and $P_{ES.dis}^{\min}$, respectively, represent the upper and lower limits of the energy storage discharging power, η_{ES}^{cha} represents the energy storage charging efficiency, η_{ES}^{dis} represents the energy storage discharging efficiency, and $\alpha_{H.cha} + \alpha_{H.dis} \le 1$ means to avoid charging and discharging electric energy storage at the same time.

(4) WD and PV power constraint

Wind power output constraint

$$\begin{cases} 0 \le P_{wd}^{t} \le P_{wd}^{sen} \\ 0 \le P_{wd.cur}^{t} \le P_{wd}^{sen} \\ P_{wd}^{t} + P_{wd.cur}^{t} = P_{wd}^{sen} \end{cases} \tag{22}$$

where P_{wd}^{sen} denotes the predicted value of wind power output.

Photovoltaic power output constraint

$$\begin{cases} 0 \le P_{pv}^{t} \le P_{pv}^{sen} \\ 0 \le P_{pv.cur}^{t} \le P_{pv}^{sen} \\ P_{pv}^{t} + P_{pv.cur}^{t} = P_{pv}^{sen} \end{cases} \tag{23}$$

where P_{pv}^{sen} denotes the predicted value of photovoltaic output.

3.3. Comprehensive Norm Constraint

In practical operations, the output of renewable energy is subject to uncertainties due to varying weather conditions. Although historical experimental data can provide a probability distribution for its output fluctuations, limitations exist in obtaining an accurate scenario of probability distribution due to data constraints. Therefore, it becomes essential to establish a suitable uncertainty set that aligns the scenario probability closer to actual conditions while fluctuating within a reasonable range. This paper proposes constructing

a confidence set based on comprehensive norms to confine the fluctuation range of the probability distribution, thereby forming an uncertainty set for renewable energy output. By creating a confidence interval rooted in comprehensive norms, it constrains the fluctuation scope of the scenario distribution probability, aiming to seek the optimal solution within the worst-case uncertainty set in this scenario.

(1) Constraining the probability distribution values of discrete scenarios with the initial probability distribution as the center and using the 1-norm and ∞-norm as constraint conditions result in respective feasible domains Ω_1 and Ω_∞.

$$\Omega = \begin{cases} p_i \geq 0 \quad i = 1, 2, \ldots K \\ \sum_{i=1}^{K} p_i = 1 \\ \Pr\left\{ \sum_{i=1}^{K} \left| p_i - p_i^0 \right| \leq \theta_1 \right\} \geq \alpha_1 \\ \Pr\left\{ \max \left| p_i - p_i^0 \right| \leq \theta_\infty \right\} \geq \alpha_\infty \end{cases} \tag{24}$$

where p_i denotes the scenario i probability value that needs to be updated, $\sum_{i=1}^{K} \left| p_i - p_i^0 \right| \leq \theta_1$ represents Ω_1 (1-norm), $\max \left| p_i - p_i^0 \right| \leq \theta_\infty$ represents Ω_∞ (∞-norm), θ_1 and θ_∞ represent the maximum deviation value of the probability, and α_1 and α_∞ represent the confidence of the probability distribution value.

(2) It can be seen from Reference [35] that the following confidence levels $\{p_k\}$ are satisfied:

$$\begin{cases} \Pr\left\{ \sum_{i=1}^{K} \left| p_i - p_i^0 \right| \leq \theta_1 \right\} \geq 1 - 2Ke^{-\frac{2M\theta_1}{K}} \\ \Pr\left\{ \max \left| p_i - p_i^0 \right| \leq \theta_\infty \right\} \geq 1 - 2Ke^{-2M\theta_\infty} \end{cases} \tag{25}$$

where K and M represent the number of discrete scenes and the number of sample scenes.

(3) Obtained from Equations (24) and (25)

$$\begin{cases} \theta_1 = \frac{K}{2M} \ln \frac{2K}{1-\alpha_1} \\ \theta_\infty = \frac{1}{2M} \ln \frac{2K}{1-\alpha_\infty} \end{cases} \tag{26}$$

Update probability scenario values using Equations (14)–(16) and F_1 in Equation (10).

3.4. Model Solving Method

Generally speaking, it is difficult to solve a model that combines a min–max–min structure and constraint with uncertain variables [36]. In handling uncertain variables, this paper employs a method that involves generating 10 scenarios and their corresponding probability values based on 180 days of data [37]. This is achieved through copula joint WD–PV generation and the application of the k-means clustering algorithm. The resulting probability values serve as the initial probabilities for the analysis. Current solving methods for such problems primarily include Benders' dual decomposition (BD) and the column and constraint generation algorithm (C&CG) [38]. In each iteration of BD, the optimal solution of the main problem is passed to the subproblem as a parameter. After solving the subproblem, a new optimal cut or feasibility cut is added to the main problem until the iteration process converges completely. However, the C&CG algorithm will add a new set of constraints and variables to the main problem after each iteration and approximate the optimal solution of the original problem by constantly cutting space. In contrast, the C&CG algorithm retains the second-stage continuous variables in the optimization calculation of the main problem, making the lower bound of the winner problem more compact. Therefore, the C&CG algorithm is often easier to converge than the BD method and requires fewer iterations. So, it is widely used.

4. Analysis of Numerical Examples

4.1. Model Optimization Framework

This paper separates the model from Main Problem (MP), Subproblem1 (SP1), and Subproblem2 (SP2). MP is to solve LB, SP1 is to solve $\min C'_{stage2}$. SP2 is tasked with solving $\max(p^{T+1}\min C'_{stage2})$ and $\{p_k\}$ through comprehensive norm constraints. Equations (24)–(26) are the comprehensive norm constraints.

$$\begin{cases} LB = \{\min(C_{stage1} + \eta),\ LB\} \\ UB = \left\{C_{stage1} + \max(p^{T+1}\min C'_{stage2}),\ UB\right\} \\ \eta \geq p^T C'_{stage2} \\ p^T = p^0 \quad if\ T = 1 \end{cases} \tag{27}$$

where LB represents the lower bound of the operating cost of the first stage, UB represents the upper bound of the operating cost of the second stage, p^0 represents the probability value of the initial scenario, and η represents the maximum real-time scheduling cost of the system under the limit scenario.

The model optimization process, depicted in Figure 3, involves iterative steps. Initially, based on the probability of the initial scenario, Equation (27) computes the optimal power buying (PB) considering the worst-case scenario. Subsequently, SP1 determines the most economical operational state using the equipment capacity derived from LB. Then, SP2 adjusts the probability scenario using Equations (24)–(28). In subsequent iterations, the corrected scenario probability from the previous iteration is utilized. Through iterative refinement, the residual (re) converges to the minimum value, ensuring precision.

$$re = |(UB - LB)/UB| \tag{28}$$

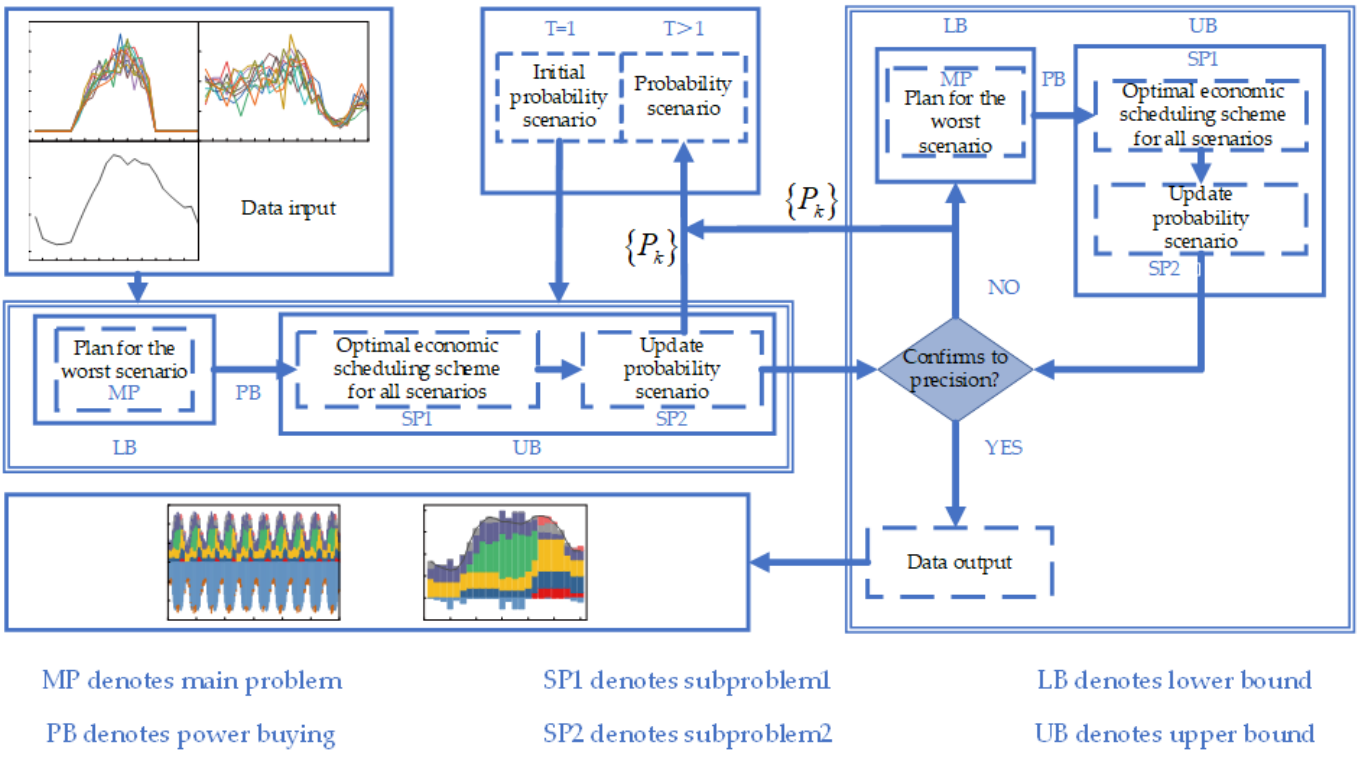

Figure 3. Model-solving flow chart.

In the first iteration, based on the initial scenario probability value, the LB of Formula (27) was calculated to obtain the best optimization scheme under the worst scenario. SP1 was

calculated according to the purchased power obtained by LB, and the optimal operating cost under the influence of the purchased power was calculated. Then, the scenario probability value was modified by $\max(p^{T+1}\min C'_{stage2})$ and Formulas (14)–(16) to calculate the worst probability distribution so as to obtain the maximum expected cost. By calculating the residual between the two, the second iteration starts with the first modified probability distribution value. Through continuous iteration, the residuals converge to the minimum, and finally the robustness and economy of the system are unified.

4.2. Introduction of Numerical Examples

To confirm the effectiveness of the model put forward, analysis and simulation were conducted on a regional power system that integrates both renewable energy sources and thermal power units. The capacity of thermal power units is 200 MW, 300 MW, and 600 MW, respectively, of which 200 MW and 300 MW units can only carry out RPR. Excepting the basic peak regulation ability, the 600 MW units can also carry out deep peak regulation after modification. The loss coefficient for the thermal power unit in deep peak shaving is 1.2, the cost of the thermal power unit is RMB 3464/kW, the fuel consumption in deep peak shaving is 4.8 t/h, and the oil price is RMB 6130/t [39]. The on–off time for units is set to 3 h, 5 h, and 8 h, respectively; The penalty cost of abandoning WD and PV is RMB 536/(MWh). The average power of the rotor cracking cycle for deep peak shaving is 240 MW. Table 1 displays additional pertinent parameters. As in Reference [6], a lithium iron phosphate battery is used for electric energy storage. The correlation coefficient is shown in Table 2, where the charge and discharge of energy storage are RMB 50/(MWh).

Table 1. Parameters associated with coal-fired thermal power units.

	Unit 1	Unit 2	Unit 3
Unit capacity/MW	200	300	600
Minimum output/%	50	50	50
a_i	1.94	0.45	0.32
b_i	140	140	140
c_i	13,776	25,704	30,576
α_i	1.16×10^{-3}	9.37×10^{-3}	1.60×10^{-3}
β_i	8.64	7.88	6.80
γ_i	113.20	158	290.40

Table 2. Actual energy storage parameters.

Energy Storage Capacity/MW	800
Self-discharge rate δ_{ES} (%)	0.05
Efficiency of charge and discharge η_{ES}^{cha}, η_{ES}^{dis}	0.95
Upper and lower limits	0.1, 0.9
Initial charge state	0.25
Max and min values of energy storage charging power $P_{ES.cha}^{\min}$, $P_{ES.cha}^{\max}$	0, 0.25
Max and min values of energy storage discharging power $P_{ES.dis}^{\min}$, $P_{ES.dis}^{\max}$	0, 0.25

Figure 4 illustrates the typical daily electricity load demand of the system. Upon observing the figure, it is evident that the system's load demand experiences significant fluctuations primarily between 10 and 17 h, with some variability around midnight. The forecasted output values of WD and PV are depicted in Figure 5, while Table 3 provides the power purchase prices set by the power grid. To examine the scheduling of all peak-load resources within the system over the course of a day, the scheduling period is configured as 10 scenarios, with each spanning 24 h with one-hour steps.

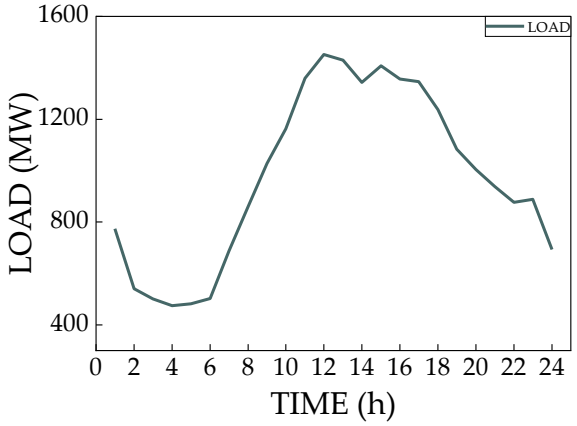

Figure 4. Electrical load demand of the system.

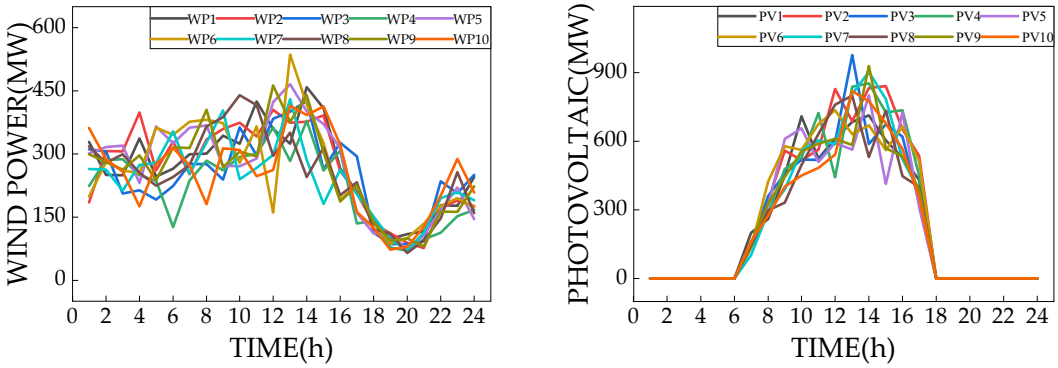

(**a**) Wind Power (**b**) Photovoltaic Power

Figure 5. Forecast of WD and PV.

Table 3. Purchase price of power grid.

Time/h	1–7	8–11	12–14	15–18	19–22	23–24
Power purchase Price/RMB/kWh	0.40	0.75	1.20	0.75	1.20	0.40

In the simulation analysis, the model built is a mixed integer linear programming problem, so this paper uses the Yalmip toolbox to call commercial solver Cplex Ver 12.1 and Gurobi Ver 9.1 in MATLAB 2021b to simulate the solution, and the computer parameters are Inter (R) Core (TM) i7 2.6 GHz and 16 GB RAM.

4.3. Analysis of Simulation Outcomes

4.3.1. Analysis of Scheduling Outcomes

To validate the economic efficiency of the model proposed in this paper, the influence of uncertainty parameter fluctuation on the total cost is considered, and the confidence levels α_1 and α_∞ of the comprehensive norm fuzzy set are 0.5 and 0.99, respectively. Taking into account the uncertainty associated with WD–PV power and load, the overall cost of the system amounts to RMB 2,651,749. This includes the generation cost of unit 1 at RMB 309,335, unit 2 at RMB 868,319, and unit 3 at RMB 137,047. Simultaneously, the carbon emissions for the entire power system total 28,199,125 t. Further detailed costs and calculation results can be found in Table 4.

Table 4. (a) Related costs of thermal power units. (b) Other relevant calculation results.

(a)			
	Unit 1	**Unit 2**	**Unit 3**
Cost of coal	RMB 295,335	RMB 854,319	RMB 1,909,841
On–off cost	RMB 14,000	RMB 14,000	RMB 14,000
Life cost of shaft	×	×	RMB 733,327
Cost of throwing oil	×	×	RMB 29,424
Deep peak shaving compensates costs	×	×	RMB 1,316,545
Sum	RMB 309,335	RMB 868,319	RMB 1,370,047
(b)			
	Energy Storage Costs	**Wind and Light Cost**	**Carbon Emissions**
Total	RMB 117,850	RMB 6.09×10^{-11}	28,199,125 t

Figure 6 displays the power balance for scheduling day 2. The figure delineates the predominant patterns of photovoltaic and wind power outputs along with the concentration of outputs from different units and energy storage. The photovoltaic output primarily occurs from early morning to evening, while wind power output is prominent from midnight to evening. Thermal power unit 1 exhibits concentrated output from 17 to 24 h, unit 2 concentrates its output from 6 to 24 h, and unit 3 maintains output throughout the day, with a peak between 18 and 21 h. Regarding peak-load management, energy storage is charged during 2–6 h and 12–15 h, aligning with higher wind power output during the former period. This allows efficient absorption of wind power output by charging the energy storage. Additionally, during 12–15 h when photovoltaic output peaks, charging the energy storage effectively absorbs a substantial proportion of photovoltaic power, mitigating the likelihood of PV and WD abandonment. The energy charge and discharge operations, coupled with power purchases from the grid, are primarily concentrated between 18 and 21 h. During this period, photovoltaic power is minimal, and wind power output decreases significantly before 18:00. This synchronization enables a balanced response to the substantial load demand during this timeframe.

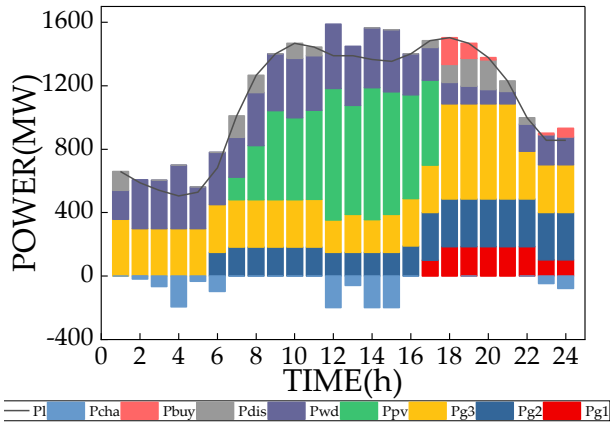

Figure 6. Power balance diagram for scheduling day 2.

4.3.2. Comparative Examination of Various Scheduling Outcomes

To validate the effectiveness of the proposed model in this paper, the following models are established for comparison:

(1) Case 1. The thermal power unit and storage deep peak shaving scheduling model proposed in this paper.
(2) Case 2. The traditional deep peak regulation scheduling model involving only thermal power units.

(3) Case 3. The three units set in this paper only carry out basic peak trimming, in which the climbing power of thermal power unit 3 is set at 50%

This paper investigates the economic impact of coordinating deep peak regulation and combined peak regulation with energy storage for thermal power units, with comparative results presented in Table 5.

Table 5. Detailed costs under the three scenarios.

Cost/RMB	Case 1	Case 2	Case 3
Cost of coal consumption	3,864,248	4,019,497	3,066,030
On–off costs	42,000	84,000	28,000
Rotating shaft life cost	733,327	499,996	×
Cost of throwing oil	29,424	176,544	×
Deep peak shaving compensates costs	1,316,544	857,142	×
Total operating cost of coal-fired units	3,352,455	3,922,894	3,094,029
Energy storage usage costs	117,850	×	81,141
Curtailment cost of WD–PV	6.09×10^{-11}	9943	2.89×10^{-11}
Combined cost	2,651,749	3,170,399	3,052,203

Among these cases, Case 2 does not incur any energy storage use cost because the energy storage does not partake in peak loading. In Case 3, there is no cost associated with rotating shaft life, oil injection, or depth peak balancing compensation because the original depth peak balancing unit operates solely in basic peak balancing mode, avoiding DPRO and, consequently, depth peak balancing compensation cost. Regarding WD and PV abandonment costs, Case 2 exhibits significantly higher expenses compared to Case 1 and Case 3. In Case 2, where energy storage is not involved in peak adjustment, surplus scenarios remain unutilized, leading to substantial waste in WD and PV generation. In terms of coal consumption costs, Case 2 surpasses Case 1 by RMB 155,249. This is because without energy storage participating in peak load balancing, thermal power units need to elevate output to absorb excess renewable energy. In Case 3, despite all units operating under RPR, the addition of energy storage significantly reduces coal consumption costs by 31.09% compared to Case 2. Regarding shaft life and fuel injection costs, Case 1 shows a higher shaft life cost by RMB 233,331 compared to Case 2. However, its fuel injection cost is RMB 147,120 lower than Case 2 because the lack of energy storage in Case 2 necessitates increased fuel consumption for DPRO to compensate for unabsorbed renewable energy. It remains crucial to prioritize turbine shaft maintenance during peak load balancing by conducting precise evaluations and real-time monitoring to mitigate damage risks. Increased investment in shaft life costs and appropriate measures are necessary to ensure stable unit operation and avert safety hazards. The electrical power balance for Case 1, Case 2, and Case 3 is illustrated in Figure 7.

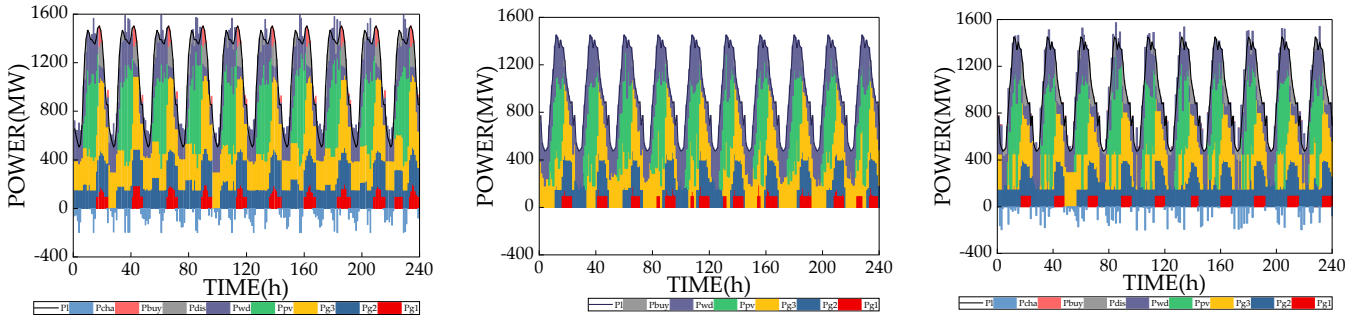

(**a**) Case 1 (**b**) Case 2 (**c**) Case 3

Figure 7. Power balance for Case 1, Case 2, and Case 3.

From Case 1 and Case 3, it is evident that the utilization of energy storage proves crucial for the deep peak shaving of thermal power units, playing a pivotal role in absorbing surplus renewable energy. While the total operating and WD–PV abandonment costs of coal-fired units in Case 3 are lower compared to Case 1, the retrofitted thermal power units in Case 3, capable of only basic peak trimming, result in significant wastage of societal resources. Additionally, upon factoring in the fuzzy set based on comprehensive norm distance, the overall cost for Case 1 is, significantly, 13% lower compared to that of Case 3. Consequently, Case 1 emerges as a more cost-effective option, exhibiting superior peak adjustment and renewable energy absorption efficacy.

Figure 8 presents a comparison between predicted and actual scenery absorption under three conditions on scheduling day 2. In Case 1 and Case 3, scenery absorption closely aligns with predictions, achieving nearly complete absorption. However, in Case 2, wind power absorption falls below the predicted value only at 4:00 and 16:00, while photovoltaic absorption lags behind the prediction at 9:00. This discrepancy arises because the energy storage in Case 2 refrains from participating in peak load regulation, allowing the system load to meet requirements during these periods, leading to the occurrence of wind and photovoltaic abandonment.

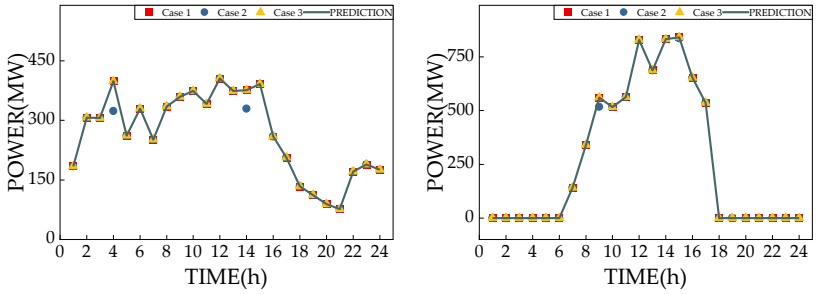

(**a**) Wind power (**b**) Photovoltaic power

Figure 8. Comparison between the prediction and the consumption situation under different conditions.

Figure 9 showcases the actual output of the three units under various scenarios, highlighting the minimum values over a span of 2 scheduling days. Unit 1 remains non-operational before 17:00, ensuring its output surpasses the minimum afterward. Similarly, unit 2 consistently maintains an output surpassing the minimum across various conditions, indicating that the basic peak shaving unit setup outlined in this paper does not lead to self-damage. In Case 3, where unit 3 is configured for basic peak load only, its actual output is not considered. However, in Case 2, unit 3 experiences shutdowns during 2–9 h and operates below its minimum output at 10:00, 12:00, 14–16 h, and 24:00. In contrast, in Case 1, unit 3 operates below the minimum output only during 12–15 h, without any shutdown occurrences. This significantly reduces the damage and associated costs incurred due to frequent operation and shutdown triggered by deep peak regulation. This further underscores the superiority and cost-effectiveness of the strategy proposed in this paper.

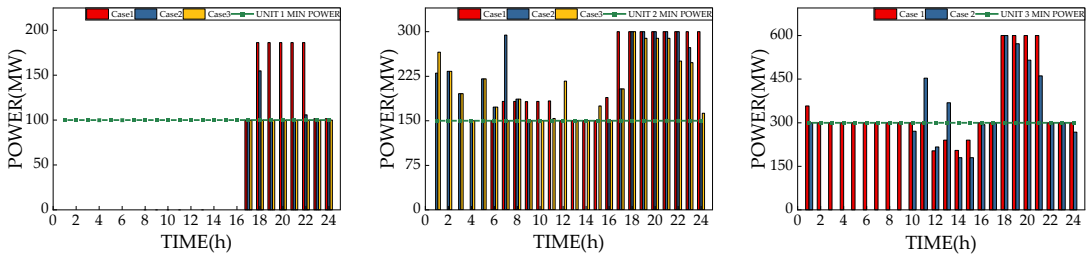

(**a**) Unit 1 (**b**) Unit 2 (**c**) Unit 3

Figure 9. Output of different units under three conditions.

4.3.3. Analysis of Results under Various Confidence Levels of the System

In distributionally robust optimization, varying confidence levels lead to different degrees of conservatism within the system. This paper examines the model's calculation outcomes by configuring diverse confidence intervals, as detailed in Table 6. In assessing the conservative response of an uncertain system, higher system costs correlate with heightened conservatism. Lower risk tolerance, on the other hand, results in larger reserve capacities adjusted by the system to counterbalance errors and energy consumption stemming from wind power and photovoltaic output [22].

Table 6. Comparison results of different confidence levels.

α_1	α_∞		
	0.50	**0.90**	**0.99**
0.20	2,669,522	2,669,522	2,650,137
0.50	2,678,975	2,678,975	2,651,749
0.90	2,704,482	2,715,838	2,665,260

Further, we chose 1-norm α_1 = 0.2, 0.5, 0.9 and ∞-norm α_∞ = 0.5, 0.9, 0.99, respectively, to compare with the comprehensive norm constraints, as shown in Table 7(a,b). The outcomes indicate that, at the equivalent confidence level, the operational cost of the comprehensive norm is lower than that of the single norm constraint.

Table 7. (a) Comparison results of synthetic norm and 1-norm constraint. (b) Comparison results of synthetic norm and ∞-norm constraint.

(a)		
	Synthetic Norm	**1-Norm**
0.20	2,650,137	2,669,522
0.50	2,651,749	2,678,975
0.90	2,665,260	2,715,999
(b)		
	Synthetic Norm	**∞-Norm**
0.50	2,678,975	2,730,154
0.90	2,678,975	2,737,222
0.99	2,651,749	2,665,260

4.3.4. Comparison of System Carbon Emissions

The inflexibility of the power system poses challenges when confronted with a substantial influx of new energy, particularly in scenarios characterized by small loads and high WD–PV power generation. This situation necessitates frequent operation of coal-fired units at low loads, leading to increased unit coal consumption, diminished system operational efficiency, and heightened carbon emissions. Hence, studying the power system's carbon emissions concerning new energy becomes immensely significant. Table 8 provides a breakdown of carbon emissions from Case 1 to Case 3.

Table 8. Comparison of carbon emission intensity in the three scenarios.

	Case 1	**Case 2**	**Case 3**
Carbon emissions/t	28,199,125	29,525,768	32,411,404

As observed in Table 8, the carbon emissions in Case 1 are 4.49% lower than those in Case 2 and 8.90% lower than those in Case 3, respectively. Consequently, the scheduling strategy proposed in this paper demonstrates lower carbon emissions compared to the

strategy combining thermal power unit and energy storage for peak shaving. This approach is notably more environmentally friendly.

5. Conclusions

In this study, we propose a distributionally robust optimal scheduling strategy for a WD–PV thermal storage power system while considering the deep peak shaving of thermal power units. This strategy harnesses the full potential of both conventional thermal power and deep peak shaving units, alongside the flexible utilization of electrical energy storage systems to integrate renewable energy. We introduce a data-driven, distributionally robust optimization approach to solve the uncertainties inherent in renewable energy sources, achieving a synergistic optimization of system robustness and economic efficiency. The efficacy of the proposed strategy is demonstrated through computational examples, leading to the following conclusions:

(1) When implementing the strategy delineated in this paper, it is observed that although the economy of the total operating costs for the coal-fired power units in Case 1 is marginally less favorable than those in Cases 2 and 3, the overall economic efficiency of the system is markedly enhanced when taking into account the fuzzy set based on the comprehensive norm distance. Concurrently, the carbon emissions in Case 1 are substantially lower in comparison to Cases 2 and 3. This underscores the profound importance of the cooperative operation of coal-fired units with peak load balancing capabilities and energy storage not only for the economic and low-carbon functioning of the power system but also for the tiered utilization of energy.

(2) The deployment of DRO focusing on the comprehensive norm can strike a superior equilibrium between robustness and economic efficiency. Consequently, DRO proves to be more adept at addressing uncertainties associated with variable forces, such as those from WD and PV sources. Moreover, the dual confidence intervals of the comprehensive norm serve as key parameters that reflect the risk preferences of the decision maker. A lower degree of conservatism correlates with reduced operational costs, yet this also diminishes the robustness of the strategy. Thus, decision makers are required to select different confidence intervals that align with their varying risk appetites.

(3) It is advisable to prioritize coal-fired units with substantial capacity and a high frequency of significant load fluctuations as the focal point for emission reduction initiatives. In tandem, regular inspections of the turbine rotor are critical to promptly detect any initial cracks and address them effectively. Furthermore, it is essential to bolster investment in the lifecycle maintenance costs of the unit's rotating shaft to forestall any potential accidents.

The findings of this study offer valuable theoretical insights for the integrated peak-load scheduling of conventional thermal power units, deep peak shaving units, and energy storage, particularly when integrating new energy sources into the power system. However, this paper does not account for the investment costs associated with energy storage capacity or the carbon emissions costs related to low-carbon dispatch strategies, and the estimation of carbon emissions from coal-fired units is somewhat idealized. The forthcoming research will extend its focus to include the capacity configuration and investment cost of energy storage, aiming to maximize scheduling efficiency and economic benefits. Additionally, the impact of carbon emissions from thermal power units during peak load balancing cannot be overlooked, necessitating a thorough examination of carbon emission costs in future analyses. Furthermore, the study will account for demand response variability and uncertainty in load and explore the flexible conversion capabilities of thermal power units. Moreover, it will persist in investigating the feasibility of strategies under the integration of renewable energy sources.

Author Contributions: Writing—original draft, Z.Z.; Writing—review & editing, R.Z. All authors have read and agreed to the published version of the manuscript.

Funding: This research was funded by National Natural Science Foundation of China grant number 52167015; and funded by Key University Laboratory—Electrical Engineering Laboratory Support Project of the Department of Education of Tibet Autonomous Region grant number 2022D-ZN-01.

Data Availability Statement: Dataset available on request from the authors.

Conflicts of Interest: The authors declare no conflict of interest.

References

1. National Energy Administration. Demand Side Management Should Be Strengthened when Coal Power Reaches Peak. Available online: http://www.nea.gov.cn/2023-04/23/c_1310713059.htm (accessed on 23 April 2023).
2. Xiao, P. *Principles and Applications of Clean Energy Engineering Technology*; Tsinghua University Press: Beijing, China, 2017; pp. 145–146.
3. Yang, Y.; Zeng, Y.; Qin, C.; Wang, C. Planning model for flexibility reformation of thermal power units for deep peak regulation. *Autom. Electr. Power Syst.* **2021**, *45*, 79–88. [CrossRef]
4. Liu, S.; Shen, J. Modeling of large-scale thermal power plants for performance prediction in deep peak shaving. *Energies* **2022**, *15*, 3171. [CrossRef]
5. Meng, Y.; Cao, Y.; Li, J.; Liu, C.; Li, J.; Wang, Q.; Cai, G.; Zhao, Q.; Liu, Y.; Meng, X. The real cost of deep peak shaving for renewable energy accommodation in coal-fired power plants: Calculation framework and case study in China. *J. Clean. Prod.* **2022**, *367*, 132913. [CrossRef]
6. Cui, Y.; Zhou, H.; Zhong, W.; Hui, X.; Zhao, Y. Two-stage day-ahead and intra-day rolling optimization scheduling considering joint peak regulation of generalized energy storage and thermal power. *Power Syst. Technol.* **2021**, *45*, 10–19. [CrossRef]
7. Du, M.; Niu, Y.; Hu, B.; Zhou, G.; Luo, H.; Qi, X. Frequency regulation analysis of modern power systems using start-stop peak shaving and deep peak shaving under different wind power penetrations. *Int. J. Electr. Power Energy Syst.* **2021**, *125*, 106501. [CrossRef]
8. Wang, S.; Lou, S.; Wu, Y.; Cao, K.; Zhou, K. Robust optimal dispatch of large-scale wind power integration considering deep peak regulation cost of thermal power units. *Autom. Electr. Power Syst.* **2020**, *44*, 118–125. [CrossRef]
9. Li, M. Research on Combined Deep Peak Shaving Model of Integrated Thermal Power Generation and Energy Storage System under the Condition of Large-scale Wind Power Grid Connection. Master's Thesis, Northeast Electric Power University, Jilin, China, 2022.
10. Yang, B.; Cao, X.; Cai, Z.; Yang, T.; Chen, D.; Gao, X.; Zhang, J. Unit commitment comprehensive optimal model considering the cost of wind power curtailment and deep peak regulation of thermal unit. *IEEE Access* **2020**, *8*, 71318–71325. [CrossRef]
11. Zhang, J.; Zhu, L.; Wang, Y.; Sun, Y.; Yan, Z.; Zhou, B. Global sensitivity analysis and stochastic optimization of multi-energy complementary distributed energy system considering multiple uncertainties. *J. Clean. Prod.* **2023**, *389*, 136120. [CrossRef]
12. Sun, Q.; Fu, Y.; Lin, H.; Wennersten, R. A novel integrated stochastic programming-information gap decision theory (IGDT) approach for optimization of integrated energy systems (IESs) with multiple uncertainties. *Appl. Energy* **2022**, *314*, 119002. [CrossRef]
13. Li, K.; Yang, F.; Wang, L.; Yan, Y.; Wang, H.; Zhang, C. A scenario-based two-stage stochastic optimization approach for multi-energy microgrids. *Appl. Energy* **2022**, *322*, 119388. [CrossRef]
14. Lei, G.; Bramerdorfer, G.; Ma, B.; Guo, Y.; Zhu, J. Robust design optimization of electrical machines: Multi-objective approach. *IEEE Trans. Energy Convers.* **2020**, *36*, 390–401. [CrossRef]
15. Dong, Y.; Zhang, H.; Ma, P.; Wang, C.; Zhou, X. A hybrid robust-interval optimization approach for integrated energy systems planning under uncertainties. *Energy* **2023**, *274*, 127267. [CrossRef]
16. Zhang, Y.; Xie, S.; Shu, S. Multi-stage robust optimization of a multi-energy coupled system considering multiple uncertainties. *Energy* **2022**, *238*, 122041. [CrossRef]
17. Qin, G.; Yan, Q.; Kammen, D.M.; Shi, C.; Xu, C. Robust optimal dispatching of integrated electricity and gas system considering refined power-to-gas model under the dual carbon target. *J. Clean. Prod.* **2022**, *371*, 133451. [CrossRef]
18. Bertsimas, D.; Sim, M.; Zhang, M. Adaptive distributionally robust optimization. *Manag. Sci.* **2019**, *65*, 604–618. [CrossRef]
19. Zhou, R.; Min, X.; Tong, X.; Chen, R.; Li, X.; Liu, Z. Distributional robust optimization under moment uncertainty of environmental and economic dispatch for power system. In Proceedings of the CSEE, Banff, AB, Canada, 22–25 June 2015; pp. 3248–3256.
20. Zhu, G.; Lin, J.; Luo, Z.; Dai, S.; Qin, L.; Liu, C. Review of robust optimization for generation scheduling in power systems. *Proc. CSEE* **2017**, *37*, 5881–5892.
21. Xie, R.; Wei, W.; Li, M.; Dong, Z.; Mei, S. Sizing capacities of renewable generation, transmission, and energy storage for low-carbon power systems: A distributionally robust optimization approach. *Energy* **2023**, *263*, 125653. [CrossRef]
22. Cui, S.; Zhu, R.; Gao, Y. Distributionally robust optimization of an integrated energy system cluster considering the oxygen supply demand and multi-energy sharing. *Energies* **2022**, *15*, 8723. [CrossRef]
23. Song, X.; Wang, B.; Wu, Y. Distributionally Robust Unit Commitment Based on Wind Power Scenario and Electric Vehicles Charging Station. In Proceedings of the 2022 International Conference on Cyber-Physical Social Intelligence (ICCSI), Nanjing, China, 18–21 November 2022; pp. 262–267.

24. Zhang, X.; Son, Y.; Cheong, T.; Choi, S. Affine-arithmetic-based microgrid interval optimization considering uncertainty and battery energy storage system degradation. *Energy* **2022**, *242*, 123015. [CrossRef]
25. Du, M. Reaserch on Load Frequency Control Optimization of Thermal Power Unit Under Flexible Operation. Ph.D. Thesis, North China Electric Power University, Beijing, China, 2021.
26. Xu, J. Peak Shaving Strategy and Benefit Evaluation of Thermal Power Units under the Consumption of New Energy. Master's Thesis, Nanjing University, Nanjing, China, 2021.
27. Liu, J.; Zeng, D.; Tian, L.; Gao, M.; Wang, W.; Niu, Y.; Fang, F. Control strategy for operating flexibility of coal-fired power plants in alternate electrical power systems. *Proc. CSEE* **2015**, *35*, 5385–5394.
28. Yi, W.; Zhuo, L.; Jin, L. Fuel Consumption Characteristic Coefficients Identification Restricted to Basic Equations for Thermal Power Units. *Proc. CSEE* **2017**, *37*, 1151–1160.
29. Jiang, Z.; Han, Z.; Li, M. A probabilistic model for low-cycle fatigue crack initiation under variable load cycles. *Int. J. Fatigue* **2022**, *155*, 106528. [CrossRef]
30. Espinosa, S.; Cazco, D.A.; Salcedo, M.Y. Economic dispatch hydrothermal system with CO_2 emissions constraints. *IEEE Lat. Am. Trans.* **2017**, *15*, 2090–2096. [CrossRef]
31. Tan, Q.; Ding, Y. Optimal energy-saving dispatching model for thermal power considering carbon trading and its coping mode. *Electr. Power Autom. Equip.* **2018**, *38*, 175–181+188. [CrossRef]
32. Kuo, M.-T.; Lu, S.-D.; Tsou, M.-C. Considering carbon emissions in economic dispatch planning for isolated power systems: A case study of the Taiwan power system. *IEEE Trans. Ind. Appl.* **2017**, *54*, 987–997. [CrossRef]
33. Zhanpeng, Z.; Mingfei, B.; Danyang, G.; Qichao, C.; Haiyang, J. A Model for Carbon Dioxide Emission Characteristics of Coal-Fired Units for Environment-Economic Dispatch Research. *J. Shanghai Jiaotong Univ.* **2021**, *55*, 1663–1672. [CrossRef]
34. National Energy Administration. Renewable Energy Law of the People's Republic of China. Available online: http://www.nea.gov.cn/2017-11/02/c_136722869.htm (accessed on 2 November 2017).
35. Li, Y.; Han, M.; Shahidehpour, M.; Li, J.; Long, C. Data-driven distributionally robust scheduling of community integrated energy systems with uncertain renewable generations considering integrated demand response. *Appl. Energy* **2023**, *335*, 120749. [CrossRef]
36. Liu, Y.; Guo, L.; Wang, C. Economic dispatch of microgrid based on two stage robust optimization. *Proc. CSEE* **2018**, *38*, 4013–4022.
37. Oh, D.H.; Patton, A.J. Dynamic factor copula models with estimated cluster assignments. *J. Econom.* **2023**, *237*, 105374. [CrossRef]
38. Zeng, B.; Zhao, L. Solving two-stage robust optimization problems using a column-and- constraint generation method. *Oper. Res. Lett. J. Oper. Res. Soc. Am.* **2013**, *41*, 457–461. [CrossRef]
39. Wang, X.; Huang, W.; Tai, N.; Wen, L.; Fan, F. A tie-line power smoothing strategy for microgrid with heat and power system using source-load-storage coordination control. *Trans. China Electrotech. Soc.* **2020**, *35*, 2817–2829. [CrossRef]